FREEZING-INDUCED MICROSTRUCTURAL CHANGES OF COLLAGEN SCAFFOLDS

by

JEFFREY DAVID MILLER

Presented to the Faculty of the Graduate School of

The University of Texas at Arlington in Partial Fulfillment

of the Requirements

for the Degree of

MASTER OF SCIENCE IN MECHANICAL ENGINEERING

THE UNIVERSITY OF TEXAS AT ARLINGTON

December 2006

ACKNOWLEDGEMENTS

Appreciation is expressed to Dr. Bumsoo Han for his unceasing willingness to help, even on his own personal time. Appreciation is also expressed to the University of Texas at Arlington Materials Science and Engineering Department for allowing me the use of their scanning electron microscope and sputter coater, as well as Dr. Jiechao Jiang in particular for his guidance in their use.

Special appreciation is expressed to Dr. Howard J. Arnott and Martha Gracey (Center for Electron Microscopy, University of Texas at Arlington) for their extensive knowledge and assistance with scanning electron microscope sample preparation and image acquisition.

November 27, 2006

ABSTRACT

FREEZING-INDUCED MICROSTRUCTURAL CHANGES

OF COLLAGEN SCAFFOLDS

Publication No. _____

Jeffrey David Miller, M.S.

The University of Texas at Arlington, 2006

Supervising Professor: Bumsoo Han

Understanding the effects of freezing on the functional properties of tissues is critical to cryopreservation of native and artificial tissues, and prognosis after cryotherapies. Although investigations have been performed to correlate macroscopic properties such as mechanical properties with freezing parameters, the effects are typically tissue-type dependent and no physical understanding is available to explain these effects. Since the mechanical and optical properties of a tissue are based on the characteristics of its extracellular matrix (ECM), understanding and quantifying these changes could assist in predicting the response a tissue will have to freezing under different circumstances. In this study, the microstructural changes induced to a type I collagen tissue equivalent construct after freezing to different end temperatures were

visualized using macroscopic observation, as well as optical microscopy and scanning electron microscopy. The changes were then quantified using image analysis. The study found that freezing results in a thinner and transparent gel at the macroscopic level. Optical microscopy of the frozen region portrayed apparent "wrinkles" in the matrix, and scanning electron microscopy illustrated a sparser, more disorganized scaffold of fibers, though the fibers appeared to be thicker. Image analysis results indicate that freezing causes a significant increase in matrix porosity and fiber diameter.

TABLE OF CONTENTS

LIST OF ILLUSTRATIONS

Figure Page

LIST OF TABLES

Table Page

CHAPTER 1

INTRODUCTION

1.1 Background of Cryotherapy and Cryopreservation

The use of low temperature in cryotherapy and cryopreservation has been around for many years. Cryotherapy involves the use of freezing to treat malignant tissues found in different organs. Cryopreservation involves preserving tissues, both native and engineered, by freezing and thawing.

1.1.1 Cryotherapy

In the mid-1800's, scientists became interested in trying to reach and studying the effect of lower temperatures. They discovered that by mixing ice with different solutes, such as calcium chloride, they could reach temperatures as low as 223 K [1]. Thus began the pursuit of the uses of low temperature for therapeutic purposes, including for anesthesia in the mid-1800's [2] and skin diseases in the late 1800's [3].

Cryosurgery, falling under the umbrella of cryotherapy, has been studied and used since the mid-1800's [4], though plagued with problems. First generation cryosurgery, for instance, endured many complications due to the inability to track the freezing interface during cryosurgery [5]. This problem caused cryosurgery to lose its popularity for several decades. Modern cryosurgery began, arguably, in 1961 with the development of automated equipment by Cooper and Lee: probes cooled by liquid nitrogen [6]. In 1966, in Buffalo, NY, Gonder and Soanes first proposed the use of

cryotherapy to treat prostate cancer [7]. However, complications in visualizing the cryosurgical process persisted, which caused interest in cryosurgery to decline again in the 1980's.

Then, ultrasound was developed, and a resurgence in cryosurgery occurred due to the ability to monitor freezing more effectively with improved cryosurgical equipment [6]. Argon gas began to be available for cryosurgical applications and was used in gas-driven probes, which allow for the use of cryo-probes with smaller diameters. Present-day cryosurgery involves the placement of a few cryo-probes in the malignant tissue at strategic sites to enable the freezing of the entire diseased area. Ultrasound imaging assists in the accurate placement of the probes and in monitoring the freezing progress, though inaccuracy is still present. Cryosurgery has already been used to treat several types of organs, including the kidney [8], liver [9], prostate [10], breast [11], and the cardiovascular system [12-14].

Much of the work being done today to improve cryosurgery is in trying to achieve a lower cell viability from the cryosurgical procedure. Freeze-thaw cycles are used to enhance cryo-injury [6], as well as adjusting thermal parameters such as end temperature and cooling rate [15-18]. The effect of increasing the holding time and reducing the thawing rate [19-24] has also been studied. Toscano *et al.* [25] also studied the effect of eutectic formation and Kristiansen [26] studied the leakage of fluorescent dye occurring in liposomes in saline solutions. Han and associates also demonstrated the ability to increase the effective cell-killing zone surrounding the cryosurgery probe by artificially inducing eutectic formation using different salts [27-

29]. Clark and associates verified that the combination of chemotherapy agents and freezing produced better results in lowering cancer cell viability [30]. Discovering new, more effective ways to achieve maximum cancer cell destruction during cryosurgery and better ways of being able to view the cryosurgery process are still heavily studied subjects today in the cryosurgical field.

1.1.2 Cryopreservation

Cryopreservation, the ability to keep cells, tissues, and organs alive for longer periods of time through the use of low temperature, has also been studied for years and is currently still being studied extensively. There is a high demand for native and engineered tissues for transplantation surgeries, and this demand has created what has been called the "transplantation crisis" [31]. Part of the problem becomes evident upon examination of the storage time limitations on many organs. Kidneys can only be preserved for 48 to 72 hours. Livers can be stored for 30 hours, and hearts and lungs must be transplanted within 6 hours [32]. So, extensive research is being conducted to increase the shelf life of different organs.

In an attempt to decrease the deterioration rate of stored tissues, at least four different storage methods are in use today. Hypothermic storage involves slowing metabolic processes and chemical reactions by cooling biomaterials to nonfreezing temperatures. Freeze-thaw preservation techniques involve freezing a biomaterial and storing it at low temperatures. Lyophilization or freeze-drying as a preservation technique involves freezing a biomaterial and then dehydrating it by sublimation, where it can be stored at ambient temperature. Vitrification involves cooling biomaterials to

below 0^{o}C in a way that will cause it to transform into an amorphous solid for storage [33].

Challenges to effective cryopreservation are still prevalent today. In 1949, Polge and associates first reported the ability to help protect biomaterials from freezing injury during the cooling process by injecting them with cryoprotectant agents (CPA's) [33]. However, adding CPA's and removing them from biomaterials proves to still be a problem. Controlling the injury dealt to biomaterials that is caused from biophysical events (water transport and intracellular ice formation) during freezing proves to still be a problem, as well as controlling the overall temperature response instigated from the freeze/thaw process [34].

1.2 Present Status of Knowledge

Understanding the biophysics in low temperature applications, including water transport and ice formation, has been critical to many of the advancements that have been made in cryotherapy and cryopreservation. Briefly, it is a well accepted hypothesis that when cells are frozen rapidly, water is trapped within the cell and frozen there. This is known as intracellular ice formation (IIF). This phenomenon leads to cell death. When cells are frozen slowly, intracellular water evacuates over the cellular membrane in an attempt to equilibrate the temperature within and without the cell. This causes cellular dehydration. This dehydration causes the intracellular solute to be of higher concentration, which also leads to cell death [15, 35, 36]. These biophysical events can be taken into account and harnessed to help induce cellular destruction

during cryosurgery. They also must be taken into account to help maintain healthy cells/tissues/organs during cryopreservation.

Though there has been extensive progress in cryotherapy and cryopreservation due to a better understanding of the biophysical events that occur during freezing, most of the work in these areas has been focused on the viability at the cellular and tissue levels. Less work has been done in examining the post-freezing functionality of tissue, which might be associated with the extracellular matrix (ECM) microstructure, and the work that has been done to determine the mechanical property changes of native tissues at the cellular and tissue level is inconsistent and tissue-type dependent.

Van Brocklin and Ellis examined the effect of storing human extensor tendons at temperatures between -10 and -20^{o}C and found no significant changes in the stress-strain curve or the elastic modulus [37]. Noyes and Grood found no mechanical property changes from freezing Rhesus monkey ACL's [38]. Foutz and associates found that rapid freezing does not cause a significant change in rat skin mechanical properties [39]. However, Blondel *et al.* demonstrated changes in the mechanical properties of frozen arteries. They found that strain, stress, axial force, strain energy, and wall stiffness values demonstrate the differences present between fresh and frozen arteries [40]. Grassl *et al.* froze pig arteries and showed that the physical dimensions of frozen arteries were increased, as well as the uniaxial load stiffness [41]. Viidik and Lewin [42], as well as Adam *et al.* [43], found no significant mechanical property changes in rabbit ligaments and human thoracic aortas, respectively, after freeze/thaw processes and after applying uniaxial tensile and uniaxial tensile-compression tests,

respectively. However, in examining engineered artificial tissues, others found modulus, ultimate tensile strength, and stiffness changes with differing cooling rates and end temperatures [36, 44]. Venkatasubramanian *et al.* [45] concluded that freezing affects the structure and mechanical properties of the porcine femoral artery. They found an increase in diameter, a drop in weight and a decrease in the toe region, a small change in linear modulus, and a significant increase in the average elastic modulus. However, using cryopreservation parameters caused no increase in diameter, but the toe region and linear modulus were affected. Devireddy *et al.* [36] noted that lower cooling rates caused maximum stiffness increases and strain to failure decreases in freeze/thaw samples, indicative of brittle behavior. They tried to explain this behavior as being due to collagen fibers and water contents. However, the change in fiber structure level was not performed.

1.3 Objectives and Impacts of This Study

Due to these inconsistencies and tissue-type dependencies in the research thus far, it is not well understood whether or not a frozen tissue is able to return to "normal" physiological functioning after being frozen. Though a tissue may be "alive" after freezing, it is not known whether or not it will still function as effectively as before. Such information would apply towards knowing how the body heals from a cryosurgical wound and how the body reacts to tissue that has been frozen for preservation purposes and then transplanted.

This question may be answered by understanding the microstructural changes that occur in the ECM of a tissue before and after a freeze/thaw procedure [46]. Others

have verified that the structural characteristics of the ECM are highly dependent upon its properties [47-50]. It has also been shown that the diameter and length of collagen fibers can appreciably affect the mechanical properties of the ECM, which affects the over-all mechanical properties of a tissue [51-56].

Biological tissue is essentially a deformable porous material whose pores are saturated with interstitial fluid. It is composed of cells, ECM, and interstitial fluid that fills in the micropores of the ECM. The ECM, composed primarily of collagen fibrils, is the mechanical scaffold of biological tissue. Therefore, the mechanical and optical properties of biological tissues, which affect their functionality, are essentially determined by the characteristics of the ECM structure. ECM structures differ from one another in many ways, including different sized and distributed micropores, different collagen fibril cross-linking patterns, and different interstitial fluid contents. Examining and comparing such characteristics in a tissue equivalent construct (TEC) at the ECM level before and after freezing may lead to a better understanding of how tissue reacts to the freeze/thaw conditions present in cryosurgery and cryopreservation.

In this study, the freezing-induced structural changes of collagen tissue constructs will be quantitatively investigated from macro- to micro-scales. This multi-scale investigation is performed by visualizing the collagen scaffold changes with macro- and microphotographs by optical and scanning electron microscopy after freezing/thawing the scaffold. The change will then be quantified via image analysis through calculation of the average fiber area, mean void area, and average fiber diameter.

CHAPTER 2

MATERIALS AND METHODS

2.1 Collagen Gel Preparation

The type I rat tail collagen gel solutions (Collagen I High Protein Rat Tail, Fisher Scientific, Pittsburgh, PA) were prepared according to the manufacturer's instructions (see Appendix A). Briefly, for a 2 mL tissue equivalents with a final collagen concentration of 3 mg/mL, 138 μL of sterile, ice cold 0.1 M NaOH (Sigma-Aldrich, St. Louis, MO) was added to 200 μL of warm, 10X MEM (Invitrogen, Carlsbad, CA). Next, 1062 μL of sterile, ice cold, distilled water (Invitrogen, Carlsbad, CA) was added, and the contents were mixed. Then, 600 μL of collagen with an initial concentration of 10 mg/mL was added to the solution and mixed. Finally, the solution was placed in a one-well chamber slide (Nunc Lab-Tek II Chamber Slide System, Fisher Scientific, Pittsburgh, PA) and incubated for 30 minutes at 37^{o}C and 5% CO_2 environment. After incubation, either 1X PBS was added to the samples to avoid dehydration until the freezing procedures were enacted, or the freezing procedures were enacted immediately without the addition of PBS.

2.2 Sample Freezing Procedures

The freezing of the samples was carried out on a Directional Solidification Stage (DSS) [57]. After placing the sample on the DSS, the lid of the chamber slide was removed. The stage was set to cause the samples to freeze at a cooling rate of

5°C/minute. The gap between the copper blocks of the DSS was set to 6 mm. The starting temperature was 4°C, but the effects of different end temperatures were tested (-20°C and -40°C). Half of each of the samples was frozen, leaving a frozen and unfrozen section of the same sample for image comparison with a scanning electron microscope. The samples were passively thawed after freezing, and then prepared for examination with a scanning electron microscope.

2.3 Macroscopic and Optical Microscopy Image Acquisition

After freezing the samples, a CCD camera (Hitachi KP-F2A near infrared, Hitachi Kokusai Electric America, Ltd., Woodbury, NY) was used to visualize the macroscopic properties of the gel after a passive thaw. Then, light microscopy images were acquired using a light microscope (Olympus BX51, Olympus America, Center Valley, PA) and high resolution CCD camera (Olympus DP70, Olympus America, Center Valley, PA). Pictures were taken of the gel horizontally across its centerline from the unfrozen to the frozen section at 3 mm intervals using a 100X magnification.

2.4 Preparation for Scanning Electron Microscopy

2.4.1 Osmium Tetroxide Vapor Fixation

Due to the fragile nature of some specimens, a fixation technique has been used by some wherein the sample is not touched by a liquid fixative—osmium tetroxide vapor fixation [58-60]. This fixation technique proved to be effective in allowing us to be able to effectively view the collagen scaffold. Briefly, the samples are placed in a sealed chamber with an open vial of OsO_4 for 72 hours. The vapors from the open vial gradually fix the specimen.

2.4.2 Dehydration, Drying, and Coating

After vapor fixation, plugs were cut out of the samples from four column sections (see Figure 2.1): the frozen section (F4), the frozen transition section (F3), the unfrozen transition section (UF2), and the unfrozen section (UF1).

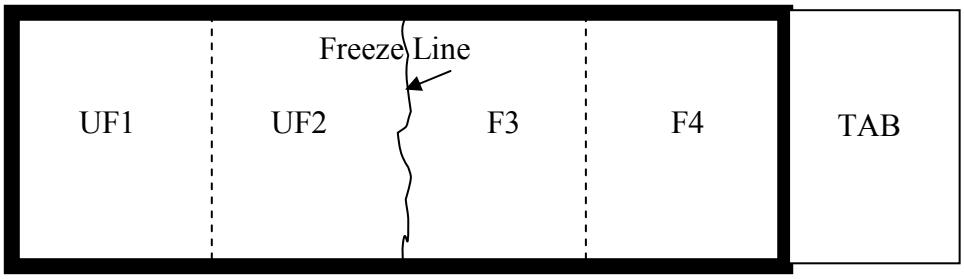

Figure 2.1 Chamber slide plug selection zones: Plugs were cut from each of the four columns to represent unfrozen, unfrozen transition, frozen transition, and frozen sections of the TEC for SEM image acquisition.

The samples were then submerged in 100% ethanol. Since collagen is notorious for retaining water, the samples were dehydrated for 72 hours. The samples were then critical point dried with a SAMDRI-PVT-3B Tousimis critical point dryer, mounted on scanning electron microscope (SEM) stubs, and coated with gold-palladium by a Hummer VI sputtering system for three minutes.

2.5 Image Acquisition and Analysis

2.5.1 Available ECM Imaging and Quantification Techniques

Visualizing the ECM structure at the microscopic level has proven to be rather difficult. Light microscopy yielded some results about a century ago when Virchow found that the orientation of collagen fibers could be visualized after interstitial injecting chromic acid [61]. Polarizing microscopy proved to be effective in visualizing

collagen fibers in the 1960s [62]. Collagen organization has been quantified using polarized light microscopy relatively recently [63, 64]. However, these techniques are ineffective at visualizing the ECM in 3-D space and at doing live-cell studies. Also, the injection of histochemical dyes requires fixatives which cause poor results. Confocal microscopy has yielded some results [65], but it is riddled with issues also, including having to cope with image artifacts and difficult optical equipment set-up. Fourier transforms have been used for 3-D quantification [66, 67], but they are limited to measurement of overall fiber orientations. The Hough transform has been used also [68, 69], but it is ineffective in measuring the curvatures of collagen fibers. Pattern matching collagen fibers is helpful with unidirectional and short fibers [70, 71], but not with long fibers in 3-D space. Wu *et al.* used 3D confocal datasets to automate the quantification and reconstruction of a collagen matrix [72], but a confocal microscope is necessary for such analysis. Our method of skeletonizing is time consuming [73, 74], but is effective in identifying individual fibers.

2.5.2 SEM Image Acquisition and Cropping

TEC images were captured using a scanning electron microscope **(**Jeol JSM-35C, Jeol Ltd., Tokyo, Japan) operating at 15 kV and using a magnification of 1500X. The images were then analyzed using IMAGEJ (http://rsb.info.nih.gov/ij) software as discussed below (also see Appendix B).

The SEM images were typically 1024X1024 pixels with the information tag (47.41 μm by 47.41 μm). These images were assessed to determine which regions were relatively flat, without uncharacteristic bright zones or clumps, and exhibiting a clear

fiber/void area. These desired regions were cropped from the original picture to a size of 130 pixels by 100 pixels (6.02 μm by 4.63 μm) (see Appendix C).

2.5.3 Fiber Diameter Measurements

In order to deduce an average fiber diameter, the length of the measure bar at the bottom of the original pictures was determined in pixels using IMAGEJ and set as a ratio of micrometers to pixels. Then, three fibers were randomly selected from each crop and their diameters in pixels was determined and converted to micrometers by multiplying them by the aforementioned ratio. An average diameter was then calculated along with a standard deviation for the unfrozen column (UF1) and the frozen column (F4) for each gel. A ratio of the frozen to unfrozen diameters was calculated for each gel and then each of these ratios were averaged for each end temperature.

2.5.4 Fiber Area Calculation

The fiber area (FA) is a measure of the area covered in an image by fiber. It was calculated as follows. The images were despeckled and then binarized using the threshold command. The images were then analyzed by examining the histogram for each image. The total number of pixels (T) and the number of black pixels (B) was noted and applied in the following equation to find the fiber area:

$$FA = \frac{B}{T} \tag{1}$$

The FA is a ratio of the black pixels in the image to the total number of pixels in the image. The meaning of this formula will be discussed more in Chapter 3.

2.5.5 Mean Void Area Calculation

The mean void area (MVA) is an estimate of the void space between fibers (porosity). Briefly, the images were despeckled, binarized with the threshold command, and then skeletonized. After attaining the histogram of the image, the total number of pixels (T) was noted, as well as the total number of white pixels (W). These were used in the following equation to determine the mean void area:

$$MVA = \frac{W}{T} \tag{2}$$

The MVA is a ratio of the white pixels in the image to the total number of pixels in the image. The meaning of this formula will be discussed more in Chapter 3.

2.5.6 Statistical Analysis

Numerous crops from different images and different gels were made in order to achieve accurate FA and MVA averages representative of a TEC. Using standard functions from Microsoft Excel, the FA and MVA calculations were averaged from all of the crops from all of the gels for each column of the TEC (see Figure 2.1), and an over-all standard deviation (SD) was calculated for each. Also, in order to better understand the standard deviation results, the percent standard deviation was calculated for the FA and MVA averages using the following formula:

$$PSD = 100 * (1 - \frac{Avg.}{Avg. + SD}) \tag{3}$$

CHAPTER 3

RESULTS AND DISCUSSION

3.1 Macroscopic Observations

A typical macroscopic photograph of a TEC after freezing/thawing is shown in Figure 3.1. The gel shown was frozen to -20°C at a cooling rate of 5°C/minute on the DSS until a black line at the top center of the chamber slide reached the -20°C block.

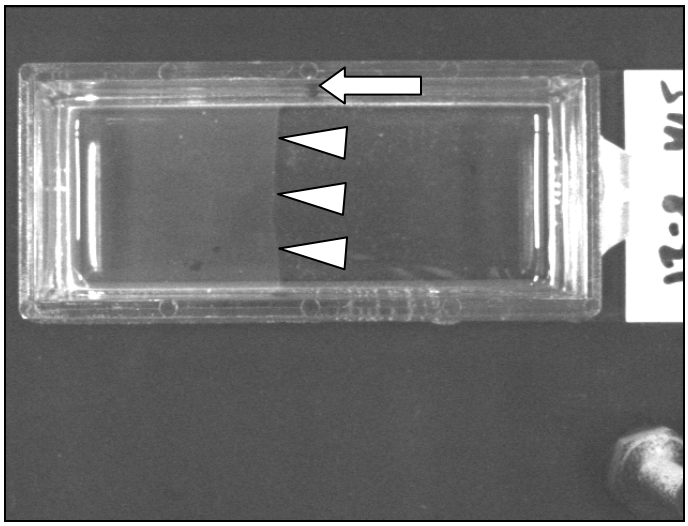

Figure 3.1 Macroscopic image of a post-frozen TEC: The right side of the chamber slide demonstrates the frozen section, and the left side is the unfrozen section. The triangular arrows point to the edge of the ice ball. The regular arrow points to the black line that stops at the edge of the low temperature block on the DSS.

As can be seen, the line indicating the edge of the ice ball (noted by the arrows) is to the left of the black line at a place that falls somewhere in between the two copper

blocks (approximately 4 mm from the -20°C block, 2 mm from the 4°C block) at the final resting place of the slide.

It is noted that there is a clear optical distinction between the frozen and unfrozen zones. The unfrozen portion is translucent, but the frozen section has become transparent. In addition to this optical distinction, macroscopic structural change is also noticed. The frozen portion of the TEC was thinner, and water was sitting on the gel. Also noted, is the fact that after approximately 30 minutes of re-incubation, the frozen section re-hydrated but did not fully recover. These observations indicate that freezing may induce a structural change in the collagen matrix of the TEC. It is this structural change that we are interested in visualizing and quantifying at the SEM level [34, 36].

3.2 Microscopic Observations Using an Optical Microscope

The typical microscopic change in TEC due to freezing to -20°C is illustrated in Figure 3.2. Using the aforementioned method, fifteen images were acquired across the centerline of the TEC, cropped, and placed side by side.

Figure 3.2 Optical microscope imaging of a TEC pre- and post-freeze: 100X magnification

The images again clearly show a microscopic structural change after a TEC is frozen. Although, the unfrozen portion of the gel remains essentially unchanged, after freezing, the gel appears to become "wrinkled." This may imply that the collagen fiber network in the frozen section is altered due to ice crystal growth during freezing. The resulting bundles of fiber may then be more visible than those in the unfrozen section.

3.3 Microscopic Observations Using a Scanning Electron Microscope

3.3.1 SEM Images of the Unfrozen TEC

Figure 3.3 exhibits representative SEM images of sections UF1 and UF2 in a TEC with a beginning temperature of 4°C and an end temperature of -20°C.

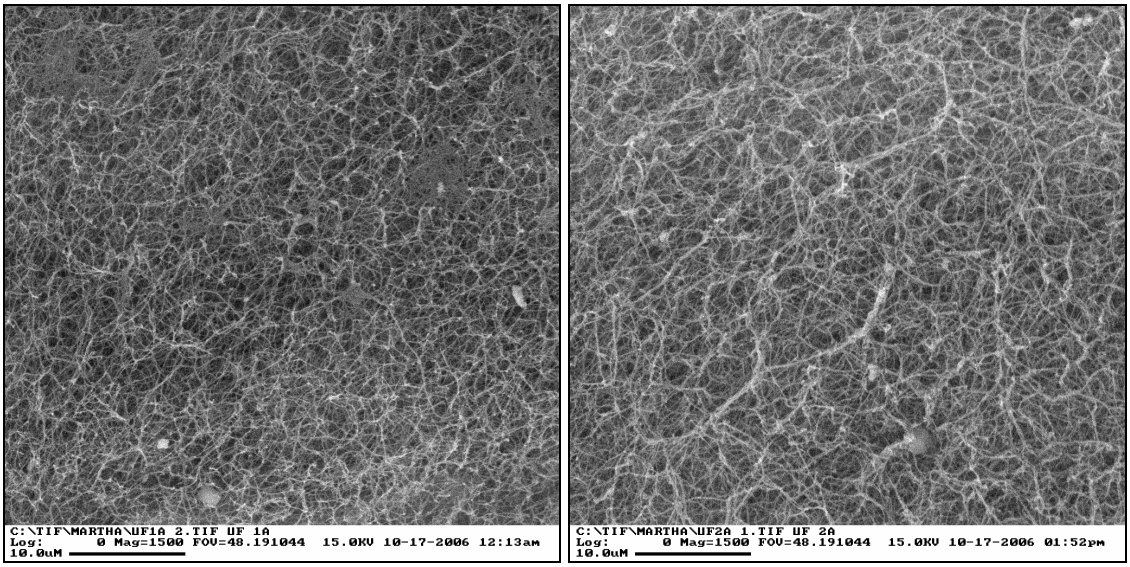

Figure 3.3 Representative unfrozen TEC SEM images: The image on the left is representative of column UF1, and the image on the right is representative of UF2. Both images are at 6% of their original size and are at 1500X magnification.

The unfrozen network of fibers (UF1) exhibits relative consistency and organization in fiber distribution and thin fibers. The scaffold is also very dense in collagen fiber concentration.

3.3.2 SEM Images of the Frozen TEC

SEM images of sections F3 and F4 in a TEC with a beginning temperature of 4^{o}C and an end temperature of -20^{o}C are exhibited in Figure 3.4.

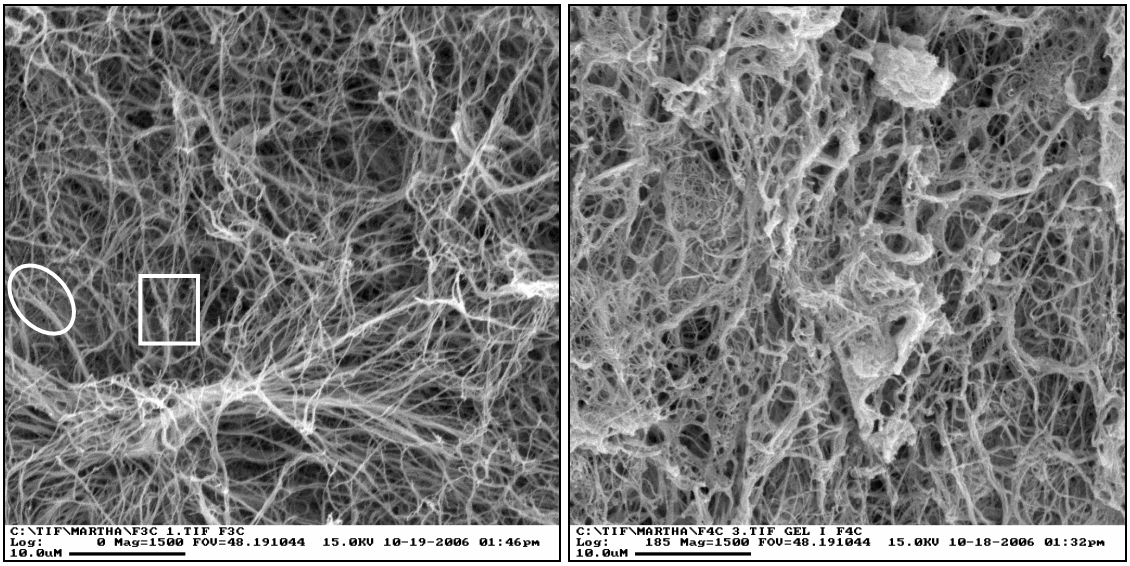

Figure 3.4 Representative frozen TEC SEM images: The image on the left is representative of column F3, and the image on the right is representative of F4. Both images are at 6% of their original size and are at 1500X magnification. Spots exhibiting fiber bundling are highlighted.

As is evident, there is an obvious structural change to the TEC post-freeze. The scaffold has expanded and the fibers are farther apart, though some of them have bunched together into bundles (highlighted areas). The individual fibers also appear to be thicker, and the scaffold has become disorganized in comparison to the scaffold displayed in the pictures of the unfrozen sections.

Also notable is the fact that some of the images that were taken of the frozen sections exhibited a thin film that had developed over the fiber structure in different places, as shown in Figure 3.5. It seems that this film-like structure corresponds to the "wrinkles" in the optical microscopic photograph. However, further research is still warranted to determine what caused the film to develop.

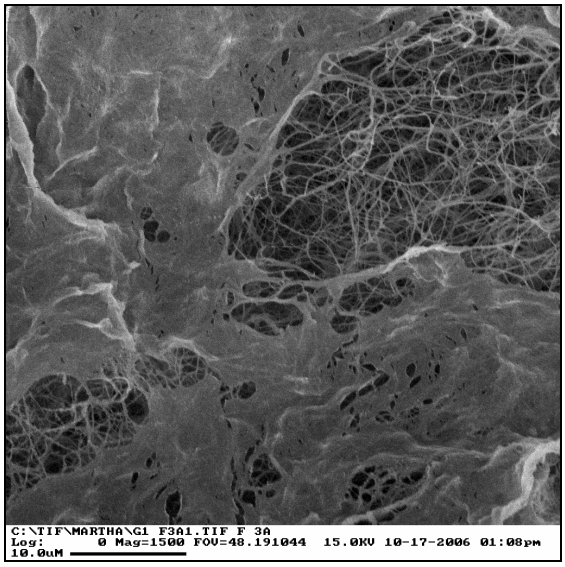

Figure 3.5 Representative SEM image of the film development over the frozen portion of a TEC: The image is at 6% of its original size and 1500X magnification.

3.4 SEM Image Analysis

3.4.1 Demonstration of the FA and MVA Acquisition Protocol

Figure 3.6 illustrates the protocol for acquiring the FA and MVA from SEM images. After opening an image in IMAGEJ, the desired representative area is cropped and then despeckled. Next, the image is binarized using IMAGEJ's automatic threshold values, and the FA is calculated using the histogram analysis option. Finally, the image

is skeletonized and the MVA is calculated with the histogram analysis option, once again.

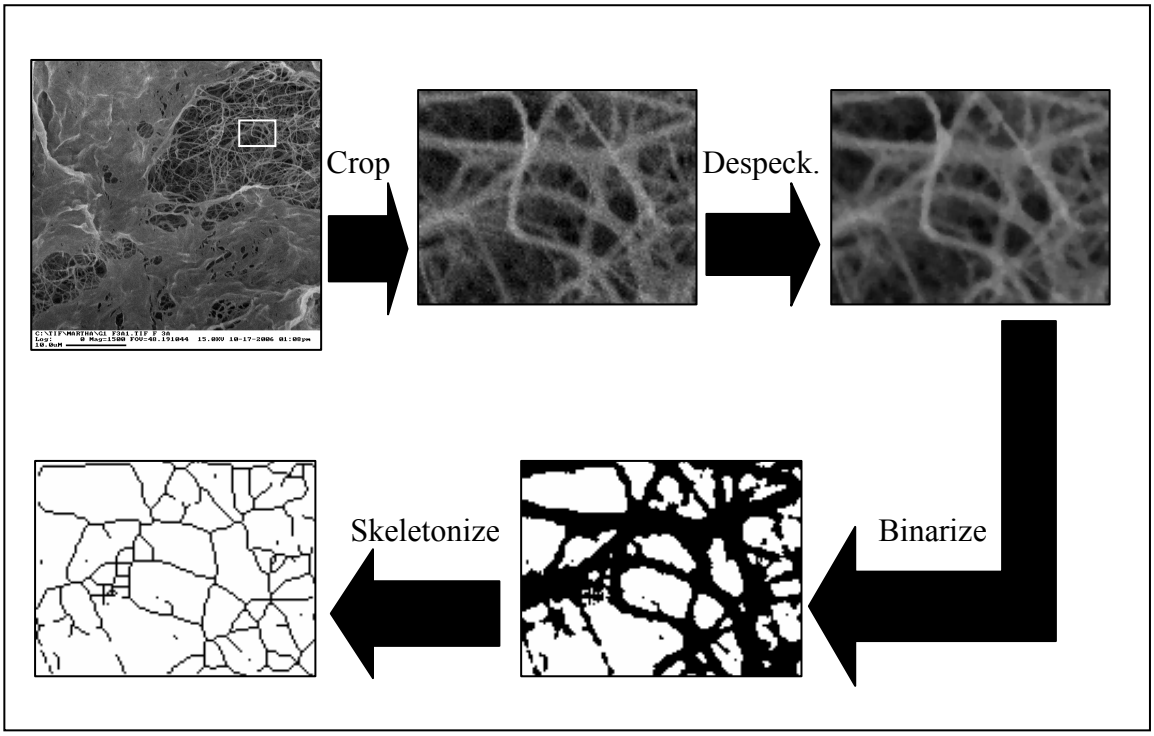

Figure 3.6 Image analysis protocol to evaluate the FA and MVA from SEM images: The cropped area is highlighted.

3.4.2 FA and MVA Results (End Temperature: -20^{o}C)

Table 3.1 summarizes the quantitative results of the image analysis from the FA, MVA, their standard deviations (SD), and percent standard deviations (%SD). Also, exhibited in the table is the number of crops that went into the calculations of each TEC column.

Table 3.1 FA and MVA Results and Standard Deviations (End Temperature: -20^{o}C)

Gel Column	FA	FA SD	FA %SD	MVA	MVA SD	MVA %SD	# of Crops
UF1	0.481	0.058	10.838	0.889	0.018	2.031	114

Table 3.1—*Continued.*

UF2	0.463	0.048	9.470	0.892	0.015	1.649	117
F3	0.471	0.065	12.071	0.912	0.014	1.560	146
F4	0.482	0.066	11.983	0.917	0.019	2.018	103

The percent standard deviation for the MVA calculations is very low (approximately 1-2%). This indicates that the resulting MVAs calculated from the crops of each column are fairly consistent—that is, the pore sizes are typically about the same size throughout the crops from that column. However, after examining and comparing the average FA percent standard deviation values for columns UF1 through F4, one can see that the percent standard deviation ranges between about 9% and 12% in the calculation of the fiber areas for each column. This indicates that the amount of area covered by fibers in each image is more sporadic/inconsistent. Some crops exhibit more fibers than others, and some crops exhibit thicker fibers than others.

Figure 3.7 (below) displays a histogram of the results from the FA calculations for the -20°C end temperature TECs.

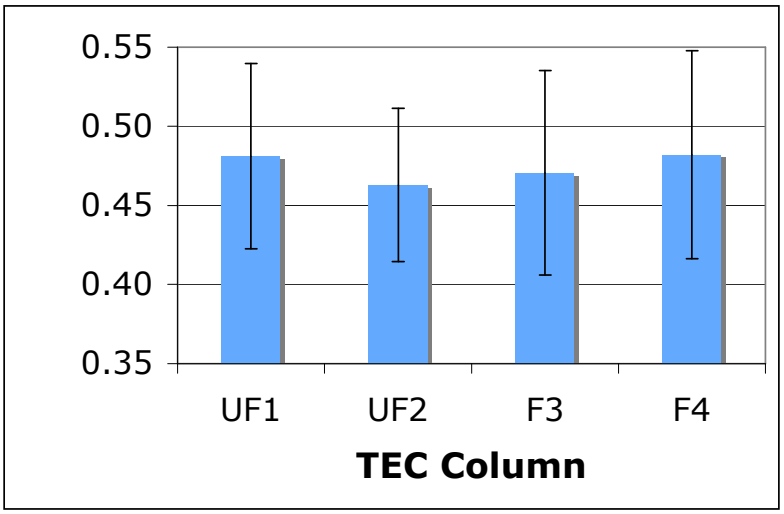

Figure 3.7 FA TEC results for an end temperature of -20°C

Notable is the fact that the FA initially decreases, and then begins to rise. The total change in fiber area from unfrozen column (UF1) to the totally frozen column (F4) ends up being not statistically significant (0.001), especially when considering the standard deviations.

A histogram of the results from the MVA calculations for the -20°C end temperature TECs is displayed in Figure 3.8.

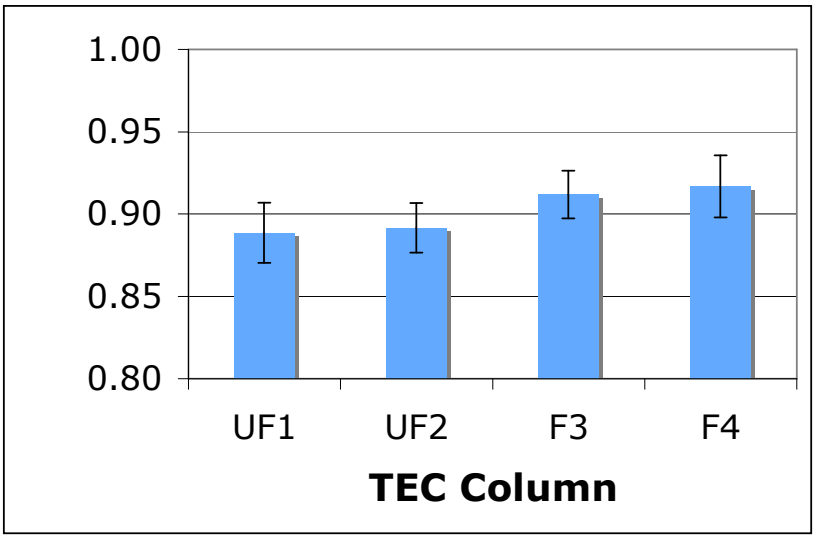

Figure 3.8 MVA TEC results for an end temperature of -20°C

Illustrated is the fact that the mean void area gradually grows through each of the columns with a jump from the unfrozen transition column to the frozen transition column. The MVA increase results in a total 2.8% growth from the unfrozen to the frozen column. This is an appreciable change since the MVA is calculated from skeletonized images with far fewer black pixels than the original images. Relatively small changes in black pixels can indicate significant fiber number changes.

Since the FA change is negligible, but the MVA is increasing, we can deduce that there must be a fiber diameter change between the unfrozen and frozen sections. This is also evident by comparing the images from the frozen and unfrozen sections with the naked eye.

3.4.3 FA and MVA Results (End Temperature: -40^{o}C)

Table 3.3 summarizes the quantitative results of the image analysis from the FA, MVA, their standard deviations (SD), and percent standard deviations (%SD). Also, exhibited in the table is the number of crops that went into the calculations of each TEC column.

Table 3.2 FA and MVA Results and Standard Deviations (End Temperature: -40^{o}C)

Gel Column	FA	FA SD	FA %SD	MVA	MVA SD	MVA %SD	# of Crops
UF1	0.473	0.059	11.029	0.890	0.027	2.975	118
UF2	0.503	0.046	8.309	0.879	0.025	2.767	120
F3	0.393	0.102	20.542	0.930	0.025	2.632	159
F4	0.431	0.091	17.433	0.927	0.020	2.077	138

The percent standard deviations for the MVA calculations are higher than those for the -20^{o}C results (approximately 2-3% rather than 1-2T). So, the MVAs of the lower temperature are less consistent. However, after examining and comparing the average FA percent standard deviation values for columns UF1 through F4, one can see that the percent standard deviation ranges between about 8% and 21% in the calculation of the fiber areas for each column, rather than the previous 9-12%. This indicates that the amount of area covered by fibers in each image is even more sporadic/inconsistent.

Some crops exhibit more fibers than others, and some crops exhibit thicker fibers than others.

Figure 3.9 (below) displays a histogram of the results from the FA calculations for the -40°C end temperature TECs.

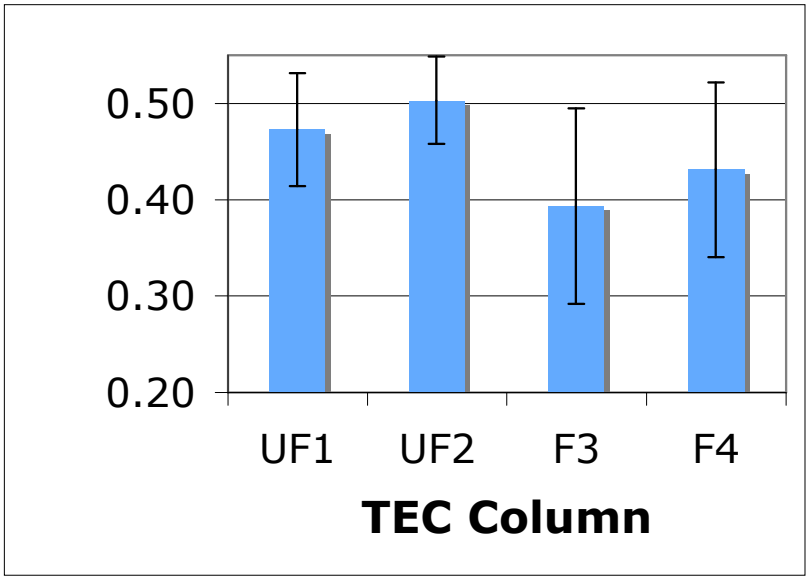

Figure 3.9 FA TEC results for an end temperature of -40°C

The FA starts at approximately the same UF1 value as the -20°C UF1 column value. However, after a freeze to -40°C, the fiber area initially increases this time, as opposed to the results from the -20°C freeze. There is then a major decrease in FA (11%) to a point some 8% below the F3 column result of the -20°C samples. The FA then rises towards the initial FA found in column UF1, as did the FA for column F4 for the -20°C samples. However, the percent standard deviations for the F3 and F4 columns are very high (21% and 17% respectively).

A histogram of the results from the MVA calculations for the -40°C end temperature TECs is displayed in Figure 3.10.

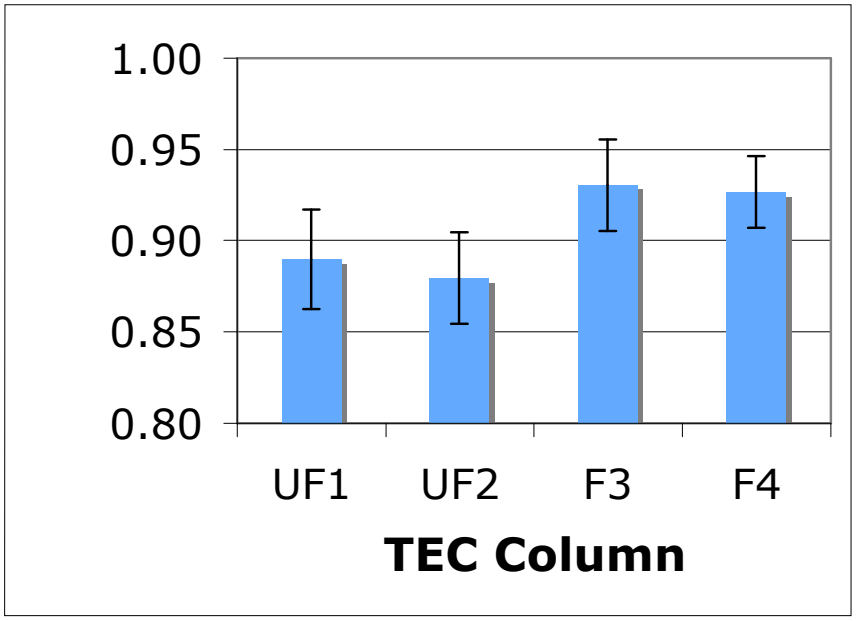

Figure 3.10 MVA TEC results for an end temperature of -40°C

Although there is initially a small decrease in the MVA, an even larger jump in MVA occurs this time across the freeze line (4%). After another small decrease, the total MVA change from UF1 to F4 is Illustrated is the fact that the mean void area gradually grows through each of the columns with a jump from the unfrozen transition column to the frozen transition column. The MVA increases a total of 3.7% from the unfrozen to the frozen column, as opposed to the 2.8% MVA change for the -20°C samples. This, again, can be considered to be appreciable change in MVA when considering the logistics of the skeletonizing process.

3.4.4 Fiber Diameter Results

Table 3.3 illustrates the specific change in fiber diameter and SD between unfrozen TEC section UF1 and frozen TEC section F4 for an end temperature of -20°C. The percent standard deviation is high, indicating that the fiber diameters are relatively inconsistent in size from fiber to fiber within an image. As was inferred, there is a fiber diameter increase after freezing.

Table 3.2 Fiber Diameter Change and Standard Deviations (End Temperature: -20°C)

Gel Column	Avg. Dia. (nm)	SD	% SD	# of Crops	# of Dia.
UF1	109.6	29.6	21.3	114	342
F4	171.7	55.4	24.4	103	309

Table 3.4 illustrates the specific change in fiber diameter and SD between unfrozen TEC section UF1 and frozen TEC section F4 for an end temperature of -40°C. The percent standard deviation for F4 column is very high (45%), indicating that the fiber diameters are very inconsistent in size from fiber to fiber within an image

Table 3.4 Fiber Diameter Change and Standard Deviations (End Temperature: -40°C)

Gel Column	Avg. Dia. (nm)	SD	% SD	# of Crops	# of Dia.
UF1	183.6	61.5	25.1	116	348
F4	452.5	375.0	45.3	137	388

Figure 3.11 illustrates the average of the column F4 to UF1 fiber diameter ratios for the two end temperatures. Freezing to a lower end temperature appears to cause the fiber diameter to increase more.

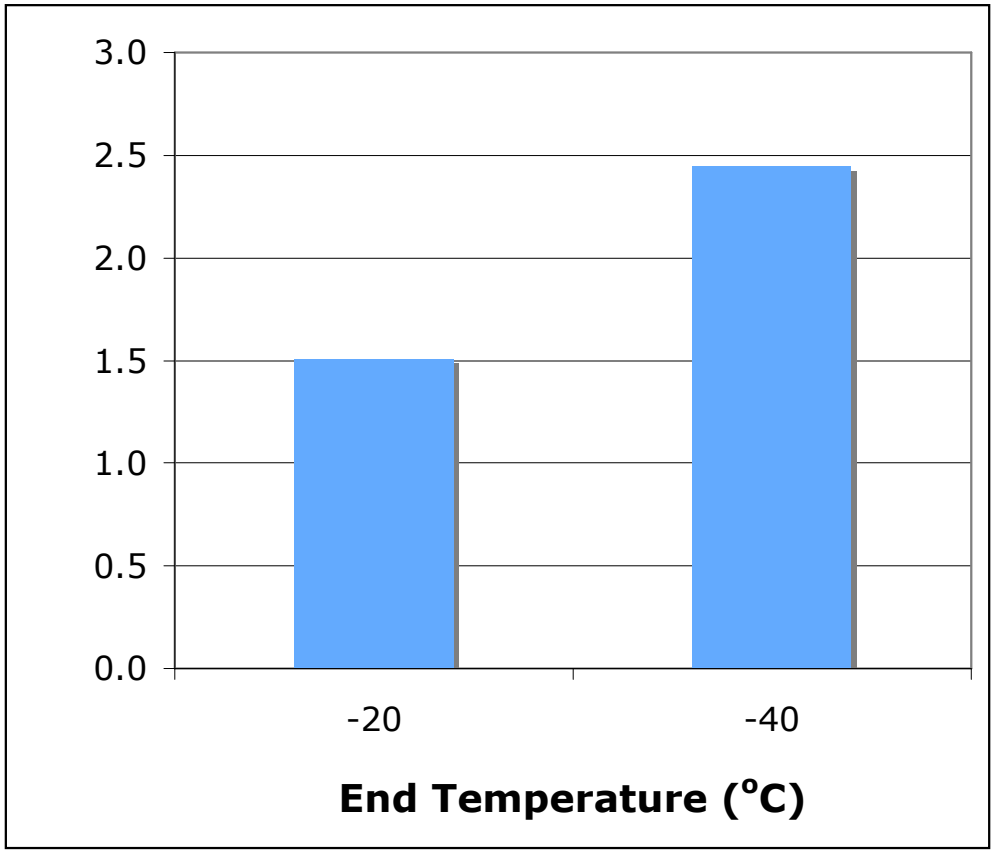

Figure 3.11 Average TEC fiber diameter ratios of column F4 to UF1 for -20°C and -40°C end temperatures

3.5 Discussion of the Results

3.5.1 Implications and Possible Applications of the Results

From the results, it is clear that a major difference between unfrozen and frozen TEC ECM structures is essentially that frozen sections are more porous than unfrozen sections. Pictures of the fiber network in frozen sections illustrate fewer fibers than unfrozen sections, but the fibers are thicker.

Re-call that after freezing, the TEC became thinner and had water residing on top of the gel. This may be contributed to by freezing-induced dehydration. Freezing a

hydrated tissue will cause a water flux due to the volumetric expansion of water [46]. This could result in tissue swelling, or perhaps, such as in this case, the evacuation of water from the tissue.

The mean void area growth through the columns and the fiber diameter growth appear to be competing against each other. An increase in MVA should decrease the FA, but an increase in fiber diameter should increase the FA. As illustrated in Figure 3.7, when freezing a TEC to -20^{o}C, the fiber area initially decreases from column UF1 to UF2, and then slightly increases in column F3. In F4, the FA increases back to approximately the value of that in UF1. It is possible that a fluid flux is initiated from columns F3 and F4 due to freezing. Water flux into the unfrozen region without fiber freezing could cause an initial growth in porosity without a fiber diameter growth, resulting in a decreased FA. Then in F3, the fibers begin to freeze, and therefore, the FA grows. Finally, the fiber thicknesses increase enough to cause the total FA change between UF1 and F4 to be statistically insignificant. However, a brief examination of the images illustrates that the growth in the pore size appears to be dominant over the fiber diameter growth. A different phenomenon could be occurring in the -40^{o}C end temperature samples. More study is required to determine the cause of those results.

The rise in the average fiber diameter could come from at least two factors. Some pictures of the frozen sections of the TEC showed a bundling of fibers, possibly due to exerted pressure on individual fibers from the expansion of ice crystals during freezing. Another possibility arises upon consideration of the structural composition of collagen fibers. Collagen fibers are hydrophilic. They are made up of bundles of fibrils

[75]. When freezing occurs, any water that is between the fibrils in collagen fibers will expand, thus causing thicker fibers.

It is widely acknowledged that pore size affects the mechanical and optical properties of a porous network [46, 76-78], such as a collagen TEC. For instance, recall that the macroscopic image of the TEC showed a change in its optical properties after freezing. The frozen portion became transparent. With the added information that the frozen portion of the TEC has larger pore sizes, it may be deduced that larger pore sizes cause the gel to become more transparent. A porous matrix that has expanded and spread its fibers out may cause fewer fiber obstructions that hinder the ability to see through the matrix.

A matrix with larger pore sizes may help in wound healing after cryosurgery, as cells will be able to more easily migrate through the matrix. The optical change that occurs after freezing may also be important for such applications as cornea transplants. After corneas have undergone cryopreservation, the freezing will have caused changes to the optical properties of their matrix. Such changes may obviously affect vision. The freezing-induced microstructural changes that occur in blood vessels after freezing could affect their mechanical strength. However, further research is necessary to ascertain how the change in fiber diameter or pore size will affect the mechanical properties of the TEC. It is uncertain whether more strands that are thinner (unfrozen region) or fewer strands that are thicker (frozen region) will be better for the mechanical properties of the TEC, if either. The answer to that question could gage the long-term response of tissue post-freezing.

3.5.2 Brief Discussion of the SEM Sample Preparation Protocol

Type I collagen gels are typically prepared for SEM examination using a basic preparation procedure [79-86]. It involves liquid fixation with glutaraldehyde, followed by osmium tetroxide fixation. Next, the samples are dehydrated with a graded ethanol series, critical point dried, and then coated with gold-palladium. The problem with the typical approach to preparing TECs for SEM observation is that the typical SEM sample preparation procedures that others use are carried out on non-frozen collagen specimens.

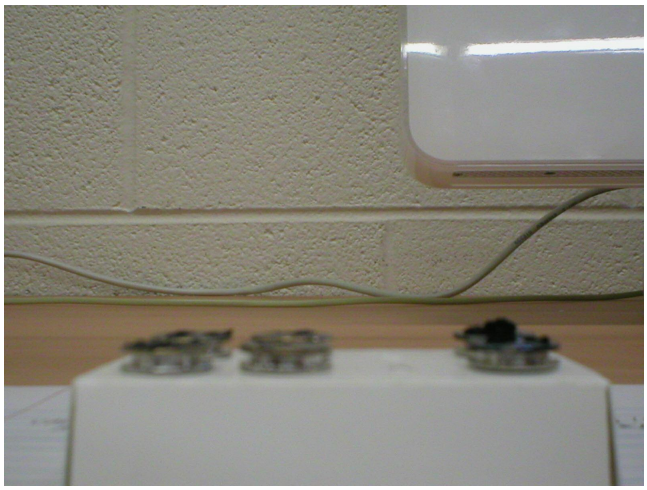

Figure 3.12 Standard verses OsO_4 fixation techniques: The samples on the left were fixed using a standard technique. The samples on the right were fixed using the OsO_4 technique.

The difference between using the typical TEC SEM sample preparation protocol (left) and vapor fixation (right) is illustrated in Figure 3.12. Utilizing the standard preparation technique resulted in a collapsed scaffold. However, using the gentler OsO_4 vapor fixation helped to maintain the structure of the TEC scaffold. The samples utilizing this technique remained "fluffy" and did not collapse.

3.5.3 Fiber Area and Mean Void Area Definition Explanation

As was articulated earlier, the fiber area is a 2-D measurement of the area covered by collagen fibers in an image. Others have used the same technique in quantifying the amount of collagen fiber present in a 3-D space (collagen density) using laser confocal microscopy [87]. The FA does not indicate how many fibers are present in a particular space, because the quantity is affected by fiber thickness also. However, coupling the information gained from the FA calculation with the MVA calculation can be beneficial in deducing more information about the TEC.

As explained above, the mean void area quantity is an estimate of the amount of void space present between the fibers in an image—that is, the porosity of the matrix viewable in a particular image. It was calculated using a procedure similar to that of Zaman *et. al.* [88]. Skeletonizing an image of a collagen network approximates each fiber in an image as a single line with a one-pixel thickness. The MVA then quantifies the amount of white pixels present in the image. The more black pixels there are in an image, the higher the number of fibers there must be in the image. Therefore, a comparison of the MVA from different images not only helps to estimate the porosity of the scaffold in a particular column of the gel, but it also helps to deduce which images have more fibers present.

The FA can then be used for more information. For instance, if the FA does not change appreciably, but the MVA does, then we can deduce that there is a change in the number of fibers present in an image. However, since the FA is not changing

appreciably, we know that the thickness of the fibers must be changing to compensate for the change in fiber numbers.

It should be noted that FA and MVA values are calculated based on 2-D images of a 3-D structure. The 3-D fibers that are being analyzed have been projected into 2-D form. Therefore, multiple layers are visible in some images, though acquiring the FA and MVA of a single layer is desired for a more accurate assessment of the TECs porosity. However, many of the fibers that are deeper in the collagen scaffold are darker due to the shadows being cast upon them from fibers that are closer to the surface of the scaffold. Many of them are, therefore, eliminated after using the threshold command of IMAGEJ, which eliminates many of the darker pixels. So, most of the fibers that are analyzed are at the surface of the collagen scaffold. This will allow us to more accurately estimate the porosity of the scaffold through calculation of the MVA.

CHAPTER 4

CONCLUSIONS

Understanding the freezing-induced microstructural changes to a collagen scaffold can have paramount implications in understanding and predicting the functional properties of tissues after freeze/thaw processes like cryotherapy and cryopreservation. In this study, certain freezing-induced structural changes to a tissue equivalent construct were identified and quantified in order to lay a foundation for further study in this area.

The following was discovered:

1) Macro-observations: Freezing caused the collagen gel matrix to change from translucent to transparent. It also became thinner, possibly due to freezing induced dehydration.
2) Micro-observations using optical microscopy: Freezing caused the gel to appear "wrinkled" at a magnification of 100X, possibly due to fibers being bundled together by the pressure from ice crystal growth in the matrix.
3) Micro-observations using scanning electron microscopy: Freezing resulted in a less organized, sparser matrix composed of thicker fibers. The fiber thickness change could be due to water expansion between the fibrils of the fibers and/or from fiber bundling.

4) Image analysis results: The mean void area, similar to a measure of porosity, increased after freezing to end temperatures of both -20^{o}C (2.8% increase from UF1 to F4) and -40^{o}C (3.7% increase from UF1 to F4) samples. The total change in fiber area pre- and post-freeze was statistically insignificant, indicative that freezing must induce a fiber diameter change. The average fiber diameter ratio from the frozen to unfrozen region was about 1.5 for TECs frozen to an end temperature of -20^{o}C and about 2.5 for an end temperature of -40^{o}C, indicating that freezing causes an increase in fiber diameter and that the lower the end temperature is, the thicker the fiber will be.

These changes to the extracellular matrix of a tissue may help to understand the mechanical and optical property changes that occur after a freeze/thaw process.

Further study is required, including:

1) The mechanical and macroscopic optical properties of a TEC should be measured and correlated to these microstructural changes.
2) Studying the results of changing the collagen content and type in a TEC is important to demonstrate the response that different tissue types will have to freezing.
3) Also, it is important to add cells to the matrix in order to more closely mimic the structure of live tissue.

These scenarios could significantly change the results acquired from the analysis of a freezing process.

APPENDIX A

PREPARATION PROTOCOL FOR A COLLAGEN GEL MATRIX

Filename: Collagen SOP Date: 11-9-06

SOP for Tissue Equivalent Construct Preparation (no cells)
(0.1 N NaOH)

I. Materials

Final Collagen Concentration: 3 (mg/mL) Initial Col. Conc.: 9.37 mg/mL

Final volume of collagen solution (in mL)

		1	2	3	4	5	6	7	8	9	10
	Location	**Amt. (mL)**	**Amt. (mL)**	**Amt. (mL)**	**Amt. (mL)**	**Amt. (mL)**	**Amt. (mL)**	**Amt. (mL)**	**Amt. (mL)**	**Amt. (mL)**	**Amt. (mL)**
10X MEM	Fridge	100	200	300	400	500	600	700	800	900	1000
Sterile 0.1 N NaOH	Fridge	74	147	221	295	368	442	515	589	663	736
Sterile dH2O	Fridge	506	1012	1519	2025	2531	3037	3543	4050	4556	5062
Rat Tail Collagen	Fridge	320	640	961	1281	1601	1921	2241	2561	2882	3202
0.1 M Hepes	Fridge	0	0	0	0	0	0	0	0	0	0
FBS	Freezer	0	0	0	0	0	0	0	0	0	0
P/S	Freezer	0	0	0	0	0	0	0	0	0	0
L- Glutamine	Freezer	0	0	0	0	0	0	0	0	0	0

II. Preparation

A. (2) 5 mL pipette

B. 1000 mL and 50 mL pipette tips

C. Chamber slides

D. 15 mL centrifuge tube

E. 1XPBS

F. Type I High Concentration Collagen

G. Container with ice cubes

III. Procedure: for 2 mL sample

NOTE: Keep NaOH and dH2O on ice until use; carry out all procedures in hood when possible

Warm bath to 37 deg. C; put on gloves; spray with ethanol

A. Warm MEM to ~37 deg. in waterbath

B. Spray inside bottom of hood with ethanol and wipe

C. Prep pipette knobs to correct sucking amount

D. Retrieve tupperware bowl, spray with ethanol and wipe, put ice in it, put it in hood, and put a 15 mL centrifuge tube in it

E. Retrieve, spray with ethanol, and wipe down NaOH and dH2O and place them in the bowl of ice in hood

F. Retrieve, wipe down, spray with ethanol, and wipe down MEM, then add to the chilled centrifuge tube (in hood) with 250 mL pipette tip

G. Add sterile, ice cold NaOH to MEM (in hood) with 250 mL pipette tip

H. Add sterile, ice cold dH2O (in hood) with 1000 mL pipette tip

I. Mix the contents of the tube by quickly pipetting several times within one minute (avoid bubbles) and hold in ice (practice needed); use 5 mL pipette.

J. Prepare the chamber slide or petri dish (retrieve, mark, and open), new 5 mL pipette, and pipette knob while the tube is on ice

K. Re-spray hands with ethanol, retrieve, spray with ethanol and wipe down collagen. Put on ice in hood.

L. Add collagen (avoid bubbles) with 1000 mL pipette tip and mix using 5 mL pipette from J.

M. Dump the mixture into chamber slide or petri dish using the same 5 mL pipette; avoid the 4 corners; Use a pipette tip to cause the solution to adhere to the base of the two long walls of the chamber slide

N. Place the solution in the incubator and allow to gel at 37oC for 30 min.

O. While in incubator, refill ice tray and put in freezer; retrieve, spray with ethanol, wipe down, and put PBS in hood. Put MEM, collagen, NaOH, and dH2O back in fridge

P. When gel is ready, add 2 mL 1XPBS (at room temperature) to cover the whole gel with 2 mm thickness (for chamber slides)

Q. Place in incubator until experiment

NOTE: Check PBS thickness periodically to avoid gel dehydration

Also, be sure to remove PBS from surface of gel before freezing, fixing, etc.

APPENDIX B

IMAGE ANALYSIS

SEM TEC Image Analysis Protocol

I. Open ImageJ, macros ("Actual 1.txt" and "Actual 2.txt"), and the desired picture

II. Click on the "Straight line selections" in the "ImageJ" window, and use it to measure the length (in pixels) of the scale bar on the image. Note how many micrometers the scale bar represents. NOTE: Some images are 1024X1024 pixels and some are 640X640. This will affect how many pixels the scale bar is in length.

III. Image > Duplicate (name it)

IV. Crop and save the desired area of the picture. NOTE: Locate areas where the layering of fibers is such that voids can be seen. Otherwise, ImageJ will not be able to correctly assess what area constitutes a void. Also, the areas should be relatively flat. Image sizes 130X100 pixels.

V. Image > Zoom > In (2 times)

VI. Again using the "Straight line selections" option, randomly measure the width of three fibers in pixels. Be sure to measure the width perpendicular to the direction the fiber is going (rather than horizontally).

VII. Convert the pixel width to micrometers using the information gained from II: # micrometers (scale bar)/# pixels (scale bar) * # pixels (fiber width) = width of fiber in micrometers

VIII. Run "Actual 1" macro on the crop

A. run("Despeckle");
B. run("Threshold");
C. run("Histogram");

[or: 1. Process > noise > despeckle
2. Process > binary > threshold
3. Analyze > histogram]

IX. NOTE: Make sure that the binarized image looks right. Sometimes, ImageJ will make the fibers white instead of black pixels. If this occurs, reject the crop and start again.

X. Jot down the total number of pixels. Then, press "list" and note the number of black pixels (value 0).

XI. Input the total number of pixels (T) and the number of black pixels (B) into the equation: Fiber Area (FA)= B/T (with EXCEL)

XII. Run "Actual 2" macro

A. run("Skeletonize");
B. run("Histogram");

[or: 1. Process > binary > Skeletonize
2. Analyze > histogram]

XIII. Note the total number of pixels. Then, press "list" and note the number of black pixels again.

XIV. Input the total number of pixels (T) and the number of black pixels (B) into the equation: Mean Void Area (MVA)= (T-B)/T (with EXCEL)

XV. After acquiring all of the desired crops for a particular section, average the FA and MVA values and find the standard deviation (SD) using the standard EXCEL function and calculate the percent standard deviation (PSD) using the following formula: $PSD = 100 * (1 - \frac{Avg.}{Avg. + SD})$

APPENDIX C

IMAGE CROPS

Crops:

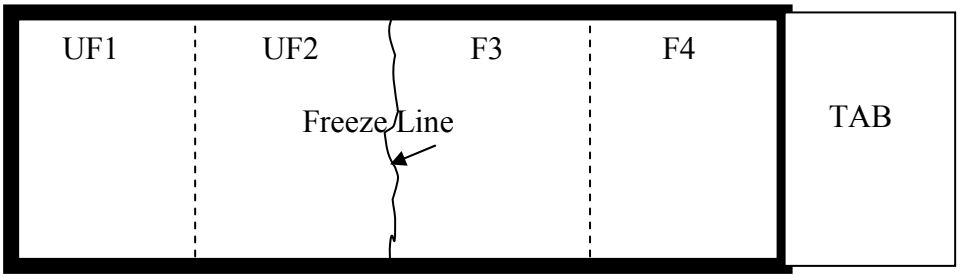

I. End Temperature: -20°C; 480 total crops

A. Sample UF1 Crops

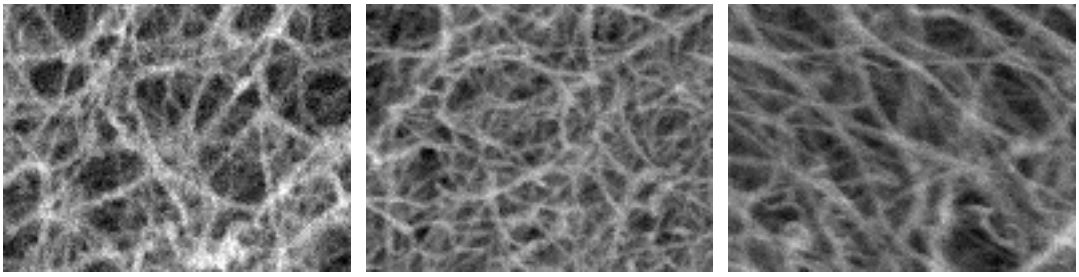

B. Sample UF2 Crops

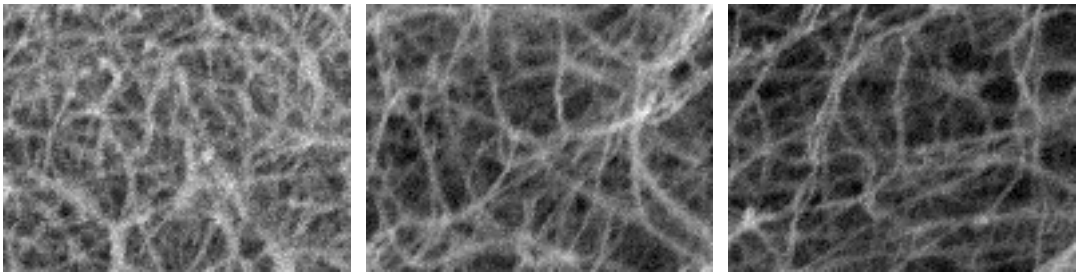

C. Sample F3 Crops

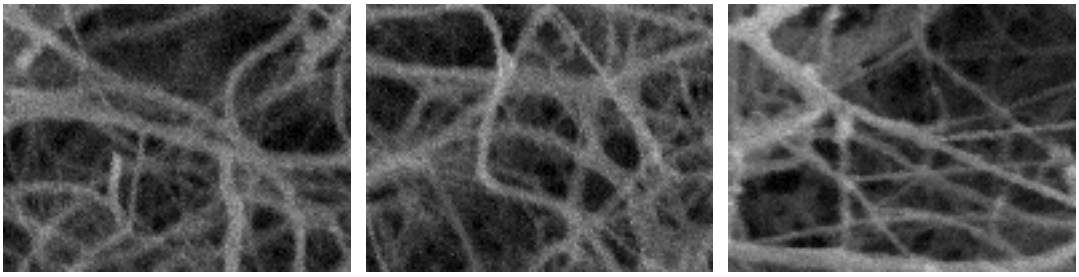

D. Sample F4 Crops

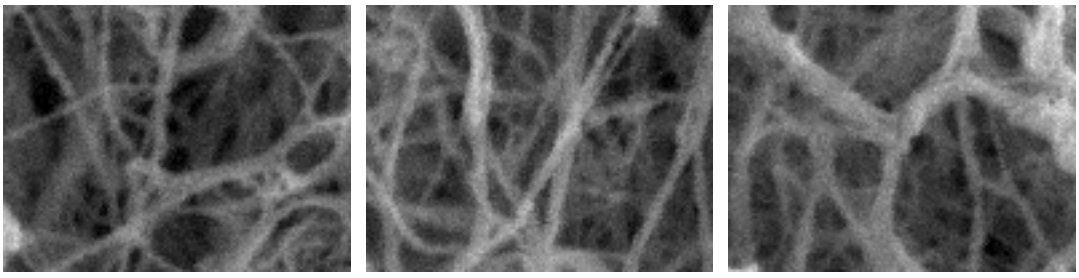

II. End Temperature: -40°C; 535 total crops

A. Sample UF1 Crops

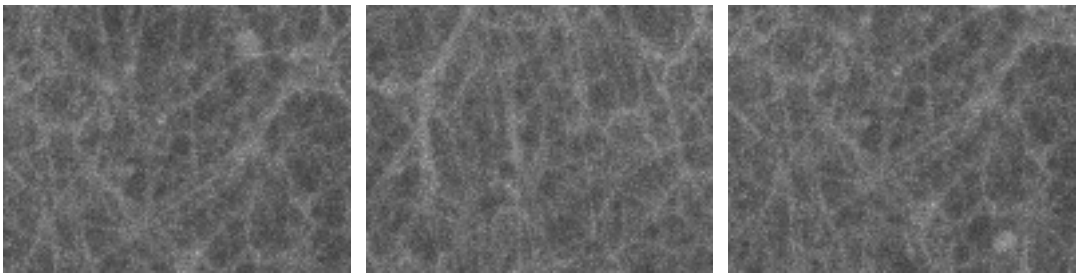

B. Sample UF2 Crops

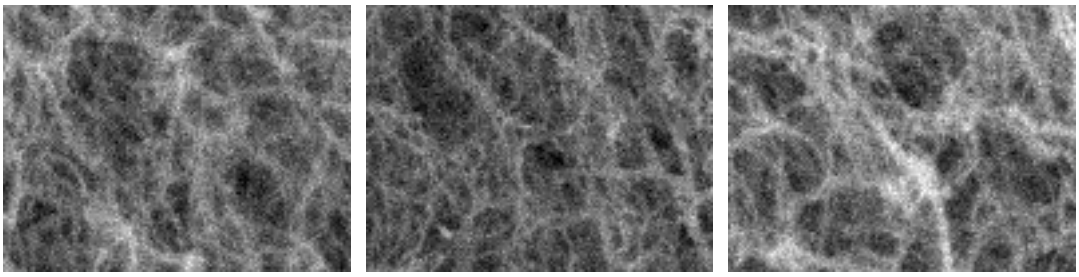

C. Sample F3 Crops

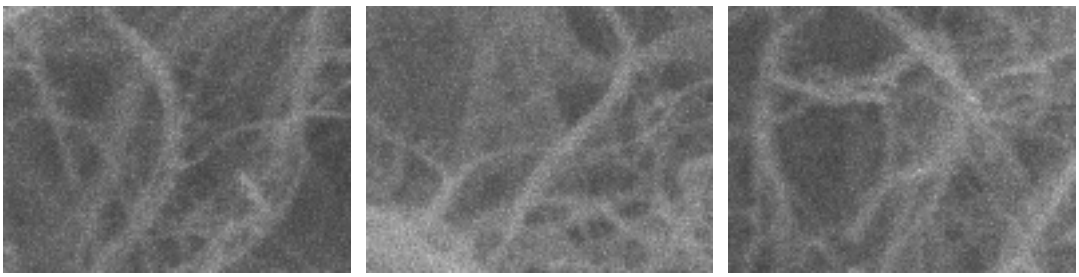

D. Sample F4 Crops

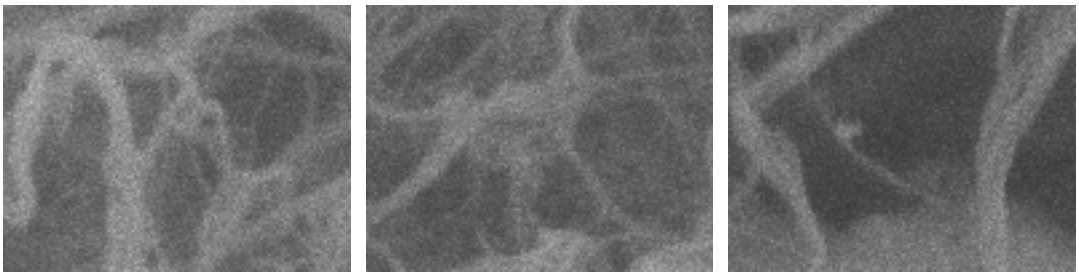

REFERENCES

[1] Arkharov, A., Marfenina, I., and Mikulin, Y., 1980, *Theory and Design of Cryogenic Systems,* Mir., Moscow, p. 430.

[2] Arnott, J., 1850, "The Remedial Efficacy of a Low Or Anaesthetic Temperature," Lancet, **2**, pp. 257.

[3] White, A. C., 1899, "Liquid Air: Its Application in Medicine and Surgery," Medical Record, **56**, pp. 109-112.

[4] Arnott, J., 1851, *On the Treatment of Cancer by the Regulated Application of an Anesthetic Temperature,* Churchill, London, p. 32.

[5] Merrick, G. S., Wallner, K. E., and Butler, W. M., 2005, "Prostate Cryotherapy: More Questions than Answers," Urology, **66**, pp. 9-15.

[6] Gage, A. A., and Huben, R. P., 2000, "Cryosurgical Ablation of the Prostate," Urologic Oncology, **5**, pp. 11-19.

[7] Fahmy, W. E., and Bissada, N. K., 2003, "Cryosurgery for Prostate Cancer," Archives of Andrology, **49**, pp. 397-407.

[8] Gill, I., and Novick, A., 1999, "Renal Cryosurgery," Urology, **54**, pp. 215-219.

[9] Seifert, J. K., Junginger, T., and Morris, D. L., 1998, "A Collective Review of the World Literature on Hepatic Cryotherapy," Journal of the Royal College of Surgeons of Edinburgh, **43**(3), pp. 141-154.

[10] Onik, G., 2003, "Focal "Nerve-Sparing" Cryosurgery for Treatment of Primary Prostate Cancer: The Male Lumpectomy?" American Journal of Oncology Review, **2**, pp. 18-24.

[11] Kaufman, C. S., and Rewcastle, J. C., 2004, "Cryosurgery for Breast Cancer," Technology in Cancer Research and Treatment, **3**, pp. 165-175.

[12] Terashima, M., 2002, "Feasibility and Safety of a Novel Cryoangioplasty System," Journal of the American College of Cardiology, **39**(Supplement A), p. 57.

[13] Kodama, T., Isobe, Y., and Kondoh, Y., 2004, "Ni/Ceramic/Molten-Salt Composite Catalyst with High-Temperature Thermal Storage for use in Solar Reforming Processes," Energy, **29**, pp. 895-903.

[14] Cheema, A. N., Nili, N., and Li, C. W., 2003, "Effects of Intravascular Cryotherapy on Vessel Wall Repair in a Balloon-Injured Rabbit Iliac Artery Model," Cardiovascular Research, **59**, pp. 222-233.

[15] Hoffmann, N. E., and Bischof, J. C., 2002, "The Cryobiology of Cryosurgical Injury," Urology, **60**(Supplement 2A), pp. 40-49.

[16] Salimi, Z., Wolverson, M. K., and Herbold, D. R., 1986, "Frostbite: Experimental Assessment of Tissue Damage using Tc-99m Pyrophosphate, Work in Progress," Radiology, **161**, pp. 227-231.

[17] Dilley, A. V., Dy, D. Y., and Warlters, A., 1993, "Laboratory and Animal Model Evaluation of the Cryotech LCS 2000 in Hepatic Cryotherapy," Cryobiology, **30**, pp. 74-85.

[18] Bourne, M. H., Piepkorn, M. W., and Clayton, F., 1986, "Analysis of Microvascular Changes in Frostbite Injury," Journal of Surgical Research, **40**, pp. 26-35.

[19] Bellman, S., and Strombeck, J. O., 1960, "Transformation of the Vascular System in Cold Injured Tissue of the Rabbit's Ear," Angiology, **11**, pp. 108-125.

[20] Artuson, G., 1966, "Capillary Permeability in Experimental Rapid Freezing with Rapid and Slow Rewarming," Acta Chirurgica Scandinavica, **131**, pp. 402-407.

[21] Bellman, S., and Adams-Ray, J., 1956, "Vascular Reactions After Experimental Cold Injury," Angiology, **7**, pp. 339-367.

[22] Entin, M. A., Schultz, G. A., and Baxter, H., 1954, "Effect of Slow and Rapid Warming on Prologoned Chilling and Freezing of the Legs of Dogs," Angiology, **5**, pp. 486-499.

[23] Hurley, L. A., 1957, "Angioarchitectural Changes Associated with Rapid Rewarming Subsequent to Freezing Injury," Angiology, **8**, p. 19.

[24] Mundth, E. D., Long, D. M., and Brown, R. B., 1963, "Treatment of Experimental Frostbite with Low Molecular Weight Dextran," Journal of Trauma, **2**, pp. 246-257.

[25] Toscano, W. M., Cravalho, E. G., and Silvares, O. M., 1975, "The Thermodynamics of Intracellular Ice Nucleation in the Freezing of Erythrocytes," Journal of Heat Transfer, **97**, pp. 326-332.

[26] Kristiansen, J., 1992, "Leakage of a Trapped Fluorescent Marker from Liposomes: Effects of Eutectic Crystallization of NaCl and Internal Freezing," Cryobiology, **29**, pp. 575-584.

[27] Han, B., and Bischof, J. C., 2003, "Enhancement of Cell and Tissue Destruction in Cryosurgery by use of Eutectic Freezing," Proceedings of SPIE Conference, **4954**, pp. 106-113.

[28] Han, B., and Bischof, J. C., 2004, "Direct Cell Injury Associated with Eutectic Crystallization during Freezing," Cryobiology, **48**, pp. 8-21.

[29] Han, B., Swanlund, D. J., and Bischof, J. C., 2003, "Enhancement of Direct Cell Injury during Freezing AT-1 Tumor Tissues by use of Eutectic Crystallization," Proceedings of 2003 ASME Summer Bioengineering Conference, , pp. 0755-0756.

[30] Clark, D. M., Baust, J. M., and van Bushkirk, R. G., 2004, "Addition of Anticancer Agents Enhances Freezing-Induced Prostate Cancer Cell Death: Implications of Mitochondrial Development," Cryobiology, **49**, pp. 45-61.

[31] Nerem, R. M., 2000, "Tissue Engineering: Confronting the Transplantation Crisis," Proc Instn Mech Engrs, **214**, pp. 95-99.

[32] Toledo-Pereyara, L.H., 1997, "Organ procurement and preservation for transplantation," Landes Bioscience, Georgetown.

[33] Coger, R., and Toner, M., 1995, *Bioengineering Handbook,* CRC Press, Boca Raton, FL, pp. 1567-1577.

[34] Han, B., and Bischof, J. C., 2004, "Engineering Challenges in Tissue Preservation," Cell Preservation Technology, **2**, pp. 91-112.

[35] Bischof, J. C., Wolkers, W. F., and Tsvetkova, N. M., 2002, "Lipid and Protein Changes with the Depth of Freezing in Dunning AT-1 Cells," Cryobiology, (In Press).

[36] Devireddy, R. V., Neidert, M. R., and Bischof, J. C., 2003, "Cryopreservation of Collagen-Based Tissue Equivalents I: Effect of Freezing in the Absence of Cryoprotective Agents," Tissue Engineering, **9**, pp. 1089-1100.

[37] Van Brocklin, J. D., and Ellis, D., 1965, "A Study of the Mechanical Behavior of Toe Extensor Tendons Under Applied Stress," Archs.Phys.Med., **46**, pp. 369-373.

[38] Noyes, F. R., and Grood, E. S., 1976, "The Strength of the Anterior Cruciate Ligament in Humans and Rhesus Monkeys," Journal of Bone and Joint Surgery, **58-A**, pp. 1074-1082.

[39] Foutz, T. L., Stone, E. A., and Abrams, C. F., 1992, "Effects of Freezing on Mechanical Properties of Rat Skin," Am J Vet Res, **53**(5), pp. 788-792.

[40] Blondel, W. C. P. M., Lehalle, B., and Maurice, G., 2000, "Rheological Properties of Fresh and Cryopreserved Human Atreties Tested in Vitro," Rheol Acta, **39**, pp. 461-468.

[41] Grassl, E. D., Barocas, V. H., and Bischof, J. C., 2004, "Effects of Freezing on the Mechanical Properties of Blood Vessels," ASME Heat Transfer Division HTD, **375**, pp. 699-703.

[42] Viidik, A., and Lewin, T., 1966, "Changes in Tensile Strength Characteristics and Histology of Rabbit Ligaments Induced by Different Models of Postmortal Storage," Acta Orthop Scand, **37**, pp. 141-155.

[43] Adam, M., Gournier, J., and Favre, J., 1996, "Mechanical Characteristics of Fresh and Frozen Human Descending Thoracic Aorta," Journal of Surgical Research, **64**, pp. 32-34.

[44] Neidert, M. R., Devireddy, R. V., and Tranquillo, R. T., 2004, "Cryopreservation of Collage-Based Tissue Equivalents II: Improved Freezing in the Presence of Cryoprotective Agents," Tissue Engineering, **10**, pp. 23-32.

[45] Venkatasubramanian, R. T., Grassl, E. D., and Barocas, V. H., 2005, "Effects of Freezing and Cryopreservation on the Mechanical Properties of Arteries," Annals of Biomedical Engineering, **34**, pp. 823-832.

[46] Han, B., 2006, "Interaction of Freezing-Induced Water Transport with Extracellular Matrix of Biological Tissues," Proceedings of 2006 ASME Summer Bioengineering Conference, **BIO2006-157692**.

[47] Berthiaume, F., Moghe, P. V., and Toner, M., 1996, "Effect of Extracellular Matrix Topology on Cell Structure, Function, and Physiological Responsiveness: Hepatochtes Cultured in a Sandwich Configuration," FASEB Journal, **10**, pp. 1471-1484.

[48] Fitton, J. H., Dalton, B. A., and Beumer, G., 1998, "Surface Topography can Interfere with Epithelial Tissue Migration," Journal of Biomedical Materials Research, **42**, pp. 245-257.

[49] Ranucci, C. S., Kumar, A., and Batra, S. P., 2000, "Control of Hepatocyte Function on Collagen Foams: Sizing Matrix Pores Toward Selective Induction of 2-D and 3-D Cellular Morphogenesis," Biomaterials, **21**, pp. 783-794.

[50] Yannas, I. V., 2005, "Structure and Function of Naturally Occurring ECMs," MIT Lecture Notes, **2006**(November 18) , p. 16.

[51] Parry, D. A., Barnes, G. R., and Craig, A. S., 1978, "A Comparison of the Size Distribution of Collagen Fibrils in Connective Tissues as a Function of Age and a Possible Relation between Fibril Size Distribution and Mechanical Properties," Proceedings of the Royal Society B: Biological Sciences, **203**, pp. 305-321.

[52] Flint, M. H., Craig, A. S., and Reilly, H. C., 1984, "Collagen Fibril Diameters and Grlycosaminoglycan Content of Skins-Indices of Tissue Maturity and Function," Connective Tissue Research, **13**, pp. 69-81.

[53] Craig, A. S., Eikenberry, E. F., and Parry, D. A., 1987, "Ultrastructural Organization of Skin: Classification on the Basis of Mechanical Role," Connective Tissue Research, **16**, pp. 213-223.

[54] Trotter, J. A., and Koob, T. J., 1989, "Collagen and Proteoglycan in a Sea Urchin Ligament with Mutable Mechanical Properties," Cell and Tissue Research, **258**, pp. 527-539.

[55] Hsu, S., Jamieson, A. M., and Blackwell, J., 1994, "Viscoelastic Studies of Extracellular-Matrix Interactions in a Model Native Collagen Gel System," Biorheology, **31**, pp. 21-36.

[56] Derwin, K. A., and Soslowsky, L. J., 1999, "A Quantitative Investigation of Structure-Function Relationships in a Tendon Fascicle Model," Journal of Biomechanical Engineering, **121**, pp. 598-604.

[57] Wang, C., 2006, "Enhancement of Cryoinjury by use of Eutectic Crystallization of an Amino Acid Adjuvant," The University of Texas at Arlington, Arlington, TX.

[58] Coetzee, S. H., Jordaan, A., and Mpuchane, S. F., 2005, "Low Pressure Mode Combined with OsO_4 Vapor Fixation and Sputter-Coating for the Preservation of Delicate Aerial Hyphae and Conidia in the ESEM," Microscopy Research and Technique, **67**, pp. 265-270.

[59] Hazlett, L. D., and Barrett, R., 1987, "Sodium Hyaluronate Eye Drop. A Scanning and Transmission Electron Microscopy Study of the Corneal Surface," Opthalmic Rsearch, **19**(5), pp. 277-284.

[60] Smith, G. F., and Tiedt, L. R., 1991, "A Rapid, Non-Destructive Osmium Tetroxide Technique for Preparing Pollen for Scanning Electron Microscopy," Taxon, **40**(2), pp. 195-200.

[61] Virchow, H., 1910, "Graefe-Saemisch Handbuch der Gesammten Augenheilkunde," Engelmann, Leipzig.

[62] Sweat, F., Rosenthal, S. I., and Puchtler, H., 1964, "Sirius Red F3BA as a Stain for Connective Tissue," Archives of Pathology, **78**, pp. 69-72.

[63] Newton, R. H., Haffegee, J. P., and Ho, M. W., 1995, "Polarized Light Microscopy of Weakly Birefringent Biological Specimens," Journal of Microscopy, **180**, pp. 127-130.

[64] Dickey, J. P., Hewlett, B. R., and Dumas, G. A., 1998, "Measuring Collagen Fiber Orientation: A Two-Dimensional Quantitative Macroscopic Technique," Journal of Biomechanical Engineering, **120**, pp. 537-540.

[65] Dunn, A. K., Smithpeter, C., and Welch, A. J., 1996, "Sources of Contrast in Confocal Reflectance Imaging," Applied Optics, **35**, pp. 3441-3446.

[66] Pourdeyhimi, B., Ramanathan, R., and Dent, R., 1997, "Measuring Fiber Orientation in Nonwovens, Part III: Fourier Transform," Textile Research Journal, **67**, pp. 143-151.

[67] Redon, C., Chermant, L., and Chermant, J. L., 1998, "Assessment of Fiber Orientation in Reinforced Concrete using Fourier Image Transform," Journal of Microscopy, **191**, pp. 258-265.

[68] Hough, P. V. C., 1962, "Methods and Means for Recognizing Complex Patterns," (3,069,654) .

[69] Davidson, N. C., and Clarke, A. R., 1999, "Extending the Dynamic Range of Fiber Length and Fiber Aspect Ratios by Automated Image Analysis," Journal of Microscopy, **196**, pp. 266-272.

[70] Clarke, A., Davidson, N., and Archenhold, G., 1993, "Measurements of Fiber Direction in Reinforced Polymer Composites," Journal of Microscopy, **161**, pp. 69-79.

[71] Davidson, N. C., Clarke, A. R., and Archenhold, G., 1997, "Large-Area, High-Resolution Image Analysis of Composite Materials," Journal of Microscopy, **185**, pp. 233-242.

[72] Wu, J., Rajwa, B., and Filmer, D. L., 2003, "Automated Quantification and Reconstruction of Collagen Matrix from 3D Confocal Datasets," Journal of Microscopy, **210**(2), pp. 158-165.

[73] Krucinska, I., 1999, "Evaluating Fibrous Architecture of Nonwovens with Computer-Assisted Microscopy," Textile Research Journal, **69**, pp. 363-369.

[74] Pourdeyhimi, B., Ramanathan, R., and Dent, R., 1996, "Measuring Fiber Orientation in Nonwovens, Part II: Direct Tracking," Textile Research Journal, **66**, pp. 747-753.

[75] Habermehl, J., 2005, "Development and Validation of a Collagen-Based Scaffold for Vascular Tissue Engineering," Laval University, Quebec, Canada.

[76] Armatas, G. S., 2006, "Determination of the Effects of the Pore Size Distribution and Pore Connectivity Distribution on the Pore Tortuosity and Diffusive Transport in Model Porous Networks," Chemical Engineering Science, **61**(14), pp. 4662-4675.

[77] Fisher, J. P., Holland, T. A., and Dean, D., 2003, "Photoinitiated Cross-Linking of the Biodegradable Polyester Poly(Propylene Fumarate). Part II. in Vitro Degradation," Biomacromolecules, **4**, pp. 1335-1342.

[78] Ma, T., Li, Y., and Yang, S. -., 2000, "Effects of Pore Size in 3-D Fibrous Matrix on Human Trophoblast Tissue Development," Biotechnol Bioeng, **70**, pp. 606-618.

[79] Huang, G. T. -., Sonoyama, W., and Chen, J., 2006, "In Vitro Characterization of Human Dental Pulp Cells: Various Isolation Methods and Culturing Environments," Cell and Tissue Research, **324**, pp. 225-236.

[80] Zhang, W., Walboomers, X. F., and van Kuppevelt, T. H., 2006, "The Performances of Human Dental Pulp Stem Cells on Different Three-Dimensional Scaffold Materials," Biomaterials, **27**, pp. 5658-5668.

[81] Fujita, K., Komatsu, K., and Tanaka, K., 2006, "An in Vitro Model for Studying Vascular Injury After Laser Microdissection," Histochemistry and Cell Biology, **125**, pp. 509-514.

[82] Boccafoschi, F., Habermehl, J., and Vesentini, S., 2005, "Biological Performances of Collagen-Based Scaffolds for Vascular Tissue Engineering," Biomaterials, **26**, pp. 7410-7417.

[83] Chazov, E. I., Alexeev, A. V., and Antonov, A. S., 1981, "Endothelial Cell Culture on Fibrillar Collagen: Model to Study Platelet Adhesion and Liposome Targeting

to Intercellular Collagen Matrix," Proceedings of the National Academy of Sciences USA, **78**(9), pp. 5603-5607.

[84] Gille, J., Meisner, U., and Ehlers, E. M., 2005, "Migration Pattern, Morphology and Viability of Cells Suspended in Or Sealed with Fibrin Glue: A Histomorphologic Study," Tissue and Cell, **37**, pp. 339-348.

[85] Nomura, Y., Toki, S., and Ishii, Y., 2000, "Improvement of the Material Property of Shark Type I Collagen by Composing with Pig Type I Collagen," Journal of Agricultural and Food Chemistry, **48**, pp. 6332-6336.

[86] Kubo, Y., Kaidzu, S., and Nakajima, I., 2000, "Organization of Extracellular Matrix Components during Differentiation of Adipocytes in Long-Term Culture," In Vitro Cellular and Developmental Biology--Animal, **36**, pp. 38-44.

[87] Kim, A., Lakshman, N., and Petroll, W. M., 2006, "Quantitative Assessment of Local Collagen Matrix Remodeling in 3-D Culture: The Role of Rho Kinase," Experimental Cell Research, **312**, pp. 3683-3692.

[88] Zaman, M. H., Trapani, L. M., and Sieminski, A., 2006, "Migration of Tumor Cells in 3D Matrices is Governed by Matrix Stiffness Along with Cell-Matrix Adhesion and Proteolysis," Proceedings of the National Academy of Sciences, **103**(29), pp. 10889-10894.

BIOGRAPHICAL INFORMATION

Jeff Miller received his E.I.T. certification in the fall of 2005. He received a B.S. degree in Mechanical Engineering from the University of Texas at Arlington in August of 2005, as well as a B.S. in Physical Science from Freed-Hardeman University (Henderson, TN) in December of 2005 with minors in French and Mathematics. His M.S. in Mechanical Engineering with an emphasis in thermal science was received in December of 2006. He is currently pursuing a Ph.D. in Mechanical Engineering at Auburn University (Auburn, AL). Jeff plans on teaching higher education upon completing his doctoral degree.